

Sliced Multi-Marginal Optimal Transport

Samuel Cohen¹ K S Sesh Kumar² Marc Peter Deisenroth¹

Abstract

We study *multi-marginal optimal transport*, a generalization of optimal transport that allows us to define discrepancies between multiple measures. It provides a framework to solve multi-task learning problems and to perform barycentric averaging. However, multi-marginal distances between multiple measures are typically challenging to compute because they require estimating a transport plan with N^P variables. In this paper, we address this issue in the following way: 1) we efficiently solve the *one*-dimensional multi-marginal Monge-Wasserstein problem for a classical cost function in closed form, and 2) we propose a higher-dimensional multi-marginal discrepancy via slicing and study its generalized metric properties. We show that computing the sliced multi-marginal discrepancy is massively scalable for a large number of probability measures with support as large as 10^7 samples. Our approach can be applied to solving problems such as barycentric averaging, multi-task density estimation and multi-task reinforcement learning.

1. Introduction

Tools arising from the optimal transport (OT) literature (Villani, 2008; Peyré and Cuturi, 2019) allow for defining discrepancies between two probability measures, and they have been applied to generative modeling (Genevay et al., 2018; Bunne et al., 2019), physics (Peyré et al., 2016), economics (Aguech and Carlier, 2011), and graph matching and averaging (Xu et al., 2019b;a). The celebrated Wasserstein distance (Monge, 1781; Kantorovich, 1958) and its generalization on incomparable spaces, Gromov-Wasserstein (Mémoli, 2011), are often used as losses in these applications.

In this paper, we consider multi-marginal OT problems, where we measure the discrepancy between P measures (for standard OT, $P = 2$). Each measure lives on a d -

¹Centre for Artificial Intelligence, University College London, UK ²Department of Computing, Imperial College London. Correspondence to: Samuel Cohen <samuel.cohen.19@ucl.ac.uk>.

dimensional space and contains N points (also referred to as *atoms*). While OT problems are typically challenging when $d \geq 2$, simple closed-form solutions often exist in a single dimension, typically obtained via a Monge reformulation (Monge, 1781). This holds for the Wasserstein (Bonneel and Pfister, 2013) and Gromov-Wasserstein (Vayer et al., 2019) distances. For both, computational complexities amount to sorting the measures' atoms ($O(N \log N)$). These closed-form solutions are then used to define tractable distances in higher dimensions by leveraging one-dimensional projections of the considered measures on $\mathbb{R}^{d \geq 1}$ onto \mathbb{R} and averaging over a space of such projections (i.e., via slicing), retaining the $O(N \log N)$ complexity. The family of sliced-(Gromov)-Wasserstein distances has grown in recent years (Bonneel and Pfister, 2013; Vayer et al., 2019; Kolouri et al., 2019) and has been applied to generative modeling (Deshpande et al., 2019a; Kolouri et al., 2018; 2019) as well as barycentric averaging (Bonneel et al., 2015).

Gangbo and Świąch (1998) study a generalization of optimal transport that allows for comparing multiple ($P \geq 2$) measures, which is relevant for multi-task regularization, barycentric averaging (Benamou et al., 2014) and multi-target domain adaptation (Cao et al., 2019). The proposed discrepancy, *multi-marginal Wasserstein* has generalized metric properties under assumptions on the form of the multi-marginal cost (Bento and Mi, 2020). Aguech and Carlier (2011) proposed the Wasserstein barycenter problem, which lifts the concept of means on Euclidean spaces to probability spaces. They show an explicit connection between the barycenter and the multi-marginal solution of the problem proposed by Gangbo and Świąch (1998).

While these multi-marginal extensions have been thoroughly studied from theoretical standpoints, it is extremely challenging to estimate such discrepancies (Lin et al., 2019), which limits their application to toy settings (low number of measures and atoms per measure). While authors propose generalizations of the Sinkhorn algorithm (Cuturi, 2013; Benamou et al., 2014) (standard algorithm for estimating OT discrepancies), the complexity of each Sinkhorn iteration is $O(P^3 N^P)$. They, and Tupitsa et al. (2020) also propose accelerated versions of such algorithms, which, however, still scale exponentially with the number of measures. Recent works (Altschuler and Boix-Adserà, 2020; Haasler et al., 2020) study cases in which multi-marginal transport can be

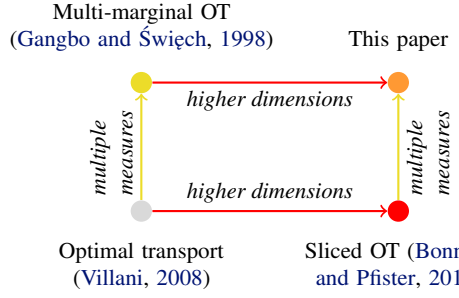


Figure 1. Diagram illustrating the contribution of our paper. We combine Sliced OT and multi-marginal OT to propose the first massively scalable OT distance between multiple measures.

efficiently solved (sometimes in polynomial time) via a low-rank structure of the cost or decomposability. They study tree-like cost structures, which enables them to leverage efficient algorithms in that setting. However, fully scalable algorithms still do not exist, hence these have not been used much in machine learning contexts.

Contributions: The main contribution of our paper is illustrated in Figure 1. We propose a multi-marginal optimal transport distance that is massively scalable. It is based on 1) a closed-form formula for the multi-marginal Monge–Wasserstein (Benamou et al., 2016) with the cost structure of Aguech and Carlier (2011) in one dimension, and 2) extending it to higher dimensions through slicing. The complexity of computing the multi-marginal distance is $O(KPN \log N)$, where K is the number of projections. This allows us to significantly extend the range of applications of multi-marginal OT distances. We study generalized metric properties (Bento and Mi, 2020) of the proposed sliced distance and prove that the sliced multi-marginal Monge–Wasserstein is a generalized metric on the space of measures of study. Finally, the potential of multi-marginal distances has not been exploited in machine learning applications because of its computational burden in previous approaches. We thus aim to propose different problems and areas where a scalable multi-marginal distance can be useful, which includes multi-task density estimation, multi-task reinforcement-learning and measure averaging.

2. Multi-Marginal Optimal Transport

2.1. Optimal Transport Between Pairs of Measures

Let $\mathcal{M}(\mathcal{X}), \mathcal{M}(\mathcal{Y})$ be the spaces of probability measures living on metric spaces \mathcal{X}, \mathcal{Y} , and $T_{\#} : \mathcal{M}(\mathcal{X}) \rightarrow \mathcal{M}(\mathcal{Y})$ be the push-forward operator. In particular, for all measurable sets $A \subset \mathcal{Y}$ and measures $\mu \in \mathcal{M}(\mathcal{X})$

$$T_{\#}\mu(A) = \mu(T^{-1}(A)). \quad (1)$$

Monge–Wasserstein Distance For a metric $d_{\mathcal{X}} : \mathcal{X} \times \mathcal{X} \rightarrow \mathbb{R}$ on \mathcal{X} , the (squared) 2-Monge–Wasserstein distance between probability measures $\mu_x, \mu_y \in \mathcal{M}(\mathcal{X})$ is (Monge, 1781; Villani, 2008)

$$\mathcal{W}_2^2(\mu_x, \mu_y) = \min_{T \in \mathcal{T}(\mu_x, \mu_y)} \int_{\mathcal{X}} d_{\mathcal{X}}^2(x, T(x)) d\mu_x(x), \quad (2)$$

where $\mathcal{T}(\mu_x, \mu_y)$ is the set of (Monge) maps $T : \mathcal{X} \rightarrow \mathcal{X}$ such that $T_{\#}\mu_x = \mu_y$. \mathcal{W}_2 measures the minimal expected cost of transporting mass from measure μ_x to measure μ_y .

Barycenters of Measures The \mathcal{W}_2 distance defined in Eq. (2) can be used to average P probability measures μ_1, \dots, μ_P by solving a barycentric problem of the form

$$\mu^* = \arg \min_{\mu \in \mathcal{M}(\mathcal{X})} \mathcal{F}(\mu), \quad \mathcal{F}(\mu) = \sum_{p=1}^P \beta_p D(\mu, \mu_p). \quad (3)$$

This general barycentric problem may use any discrepancy between two measures defined by $D : \mathcal{M}(\mathcal{X}) \times \mathcal{M}(\mathcal{X}) \rightarrow \mathbb{R}^+$, including \mathcal{W}_2^2 . Cuturi (2013); Benamou et al. (2014); Luise et al. (2019); Peyré et al. (2016) use Eq. (3) to average under various optimal transport discrepancies.

2.2. Generalization to Multiple Marginals

Gangbo and Święch (1998) propose a generalization of the optimal transport problem that allows for handling more than two measures. We consider P measures $\mu_1, \dots, \mu_P \in \mathcal{M}(\mathcal{X})$, and describe the 2-Monge–Wasserstein generalization, which has a specific cost structure described below (Aguech and Carlier, 2011; Benamou et al., 2016).

Multi-marginal Monge–Wasserstein The goal is to compute $\mathcal{MW}_2^2(\mu_1, \dots, \mu_P)$ defined as

$$\mathcal{MW}_2^2 = \min_{\substack{(T_2, \dots, T_P) \\ \in \mathcal{T}(\mu_1, \dots, \mu_P)}} \int_{\mathcal{X}} \sum_{p=1}^P \beta_p \|T_p(x) - S(T(x))\|^2 d\mu_1(x), \quad (4)$$

where $\mathcal{T}(\mu_1, \dots, \mu_P)$ is the set of $P-1$ Monge maps between μ_1 and each individual μ_p , $p = 1, \dots, P$, i.e. $T_p \# \mu_1 = \mu_p$, and $T_1 = I$. Also, $\beta \in \Delta_P$ (where Δ_P is the P -simplex), $T(x) = (x, T_2(x), \dots, T_P(x))$ maps points from μ_1 through individual transport maps, and $S(x_1, \dots, x_P) = \sum_{p=1}^P \beta_p x_p$ computes the Euclidean barycenter of the transported samples.

Intuitively, \mathcal{MW}_2 with this specific cost structure provides a measure of how close multiple measures are to each other by comparing them to their average under the Wasserstein geometry, which was originally motivated by the economics problem of matching for teams (Aguech and Carlier, 2011). There are nevertheless significantly more problems where

such properties are desirable. For example, sharing knowledge across agents in a reinforcement learning setting can be achieved by enforcing their trajectories to be close to their geometric average, hence sharing structure (see experiments section). Multi-marginal generalizations of OT problems are typically extremely challenging to solve because they require solving linear programs with N^P variables leading to exponential complexities in the number of measures P .

We note this is a Monge formulation of the problem originally studied by [Agueh and Carlier \(2011\)](#) and therefore an upper bound on its more studied Kantorovich formulation. However, the Monge formulation will allow us to derive a simple closed-form formula in the 1D case. This problem is always well-defined in the setting of the paper, namely uniform measures with identical number of atoms.

2.3. Sliced Optimal Transport

We introduce sliced optimal transport, which exploits projections onto 1D problems that are easier to solve. We define $\mathcal{M}^N(\mathbb{R}^d)$ as the set of discrete uniform probability measures with N atoms on \mathbb{R}^d . Any element μ of that set can be written as $\mu = \frac{1}{N} \sum_{n=1}^N \delta_{\mathbf{x}_n}$ for all $\mathbf{x}_n \in \mathbb{R}^d$. Optimal transport problems in one dimension are often significantly simpler to solve than ones in higher dimensions. For instance, computing the 2-Wasserstein between discrete measures on $\mathcal{M}^N(\mathbb{R})$ amounts to sorting, and has complexity $O(N \log N)$ where N is the number of support points:

$$\mathcal{W}^2(\mu_x, \mu_y) = \frac{1}{N} \sum_{i=1}^N |\tilde{x}_i - \tilde{y}_i|^2. \quad (5)$$

Here, $\tilde{x}_1 \leq \dots \leq \tilde{x}_n$, and $\tilde{y}_1 \leq \dots \leq \tilde{y}_n$. The Gromov–Wasserstein distance between measures in $\mathcal{M}^N(\mathbb{R})$ can also be computed in $O(N \log N)$, which amounts to sorting ([Vayer et al., 2019](#)).

Leveraging the tractability of OT in 1D, the sliced-Wasserstein distance $\mathcal{SW}_2^2(\mu_x, \mu_y)$ was proposed as

$$\frac{1}{\text{Vol}(S_{d-1})} \int_{S_{d-1}} \mathcal{W}_2^2(M_{\boldsymbol{\theta}} \# \mu_x, M_{\boldsymbol{\theta}} \# \mu_y) d\boldsymbol{\theta}, \quad (6)$$

where S_{d-1} is the d -dimensional hypersphere and $M_{\boldsymbol{\theta}}(\mathbf{x}) = \langle \mathbf{x}, \boldsymbol{\theta} \rangle$. The push-forward operator thus projects the individual measures onto \mathbb{R} on which computing the Wasserstein becomes simple using Eq. (5). This allows us to define a tractable discrepancy between measures in high dimensions. Eq. (6) can be efficiently estimated by Monte Carlo with complexity $O(KN \log N)$, where K is the number of projections $\boldsymbol{\theta}_k \sim \mathcal{U}(S_{d-1})$ (uniform measure on hypersphere):

$$\overline{\mathcal{SW}}_2^2(\mu_x, \mu_y) = \frac{1}{K} \sum_{k=1}^K \mathcal{W}_2^2(M_{\boldsymbol{\theta}_k} \# \mu_x, M_{\boldsymbol{\theta}_k} \# \mu_y). \quad (7)$$

Related Work [Vayer et al. \(2019\)](#) extended Eq. (6) to the Gromov–Wasserstein distance by leveraging a 1D formula for the Gromov–Wasserstein between measures on $\mathcal{M}^N(\mathbb{R})$. Slicing takes away rotational invariance. Thus, they propose an invariant formulation requiring to optimize on Stiefel manifolds. Typical sliced OT approaches leverage linear projections on \mathbb{R} . [Kolouri et al. \(2019\)](#) propose nonlinear projections arising from generalized Radon transforms for greater expressiveness. [Nadjahi et al. \(2020\)](#) study topological properties of sliced divergences and prove that slicing preserves metric properties of the base metric. While sliced OT has been thoroughly studied in the pairwise case ($P = 2$), slicing has, to the best of our knowledge, not been previously proposed in the multi-marginal case ($P > 2$).

3. Sliced Multi-Marginal Transport

To efficiently compute multi-marginal distances for many marginals, we first derive a closed-form formula for Monge–Wasserstein multi-marginal transport in 1D. We then extend our approach to higher dimensions through slicing. Finally we study generalized metric properties of the proposed distance. Analogously to other sliced optimal transport papers, we consider measures on $\mathcal{M}^N(\mathbb{R}^d)$, which guarantees the existence of Monge maps between pairs of measures.

3.1. Closed-Form Formulas for Multi-Marginal OT

Let \mathbb{S}_N be the set of permutations of order N . The closed-form formula derived in this section relies on the following:

Proposition 1. *If $\mu_x, \mu_y \in \mathcal{M}^N(\mathbb{R}^d)$, then any map $T \in \mathcal{T}(\mu_x, \mu_y)$ is a bijection. There exists $\sigma \in \mathbb{S}_N : \forall \mathbf{x}_i \in \text{Supp}(\mu_x), T(\mathbf{x}_i) = \mathbf{y}_{\sigma(i)}$.*

Proof. In [Peyré and Cuturi \(2019\)](#) □

Prop. 1 shows that if $\mu_1, \dots, \mu_P \in \mathcal{M}^N(\mathbb{R}^d)$, hence $\mu_p = \frac{1}{N} \sum_{i=1}^N \delta_{\mathbf{x}_i^{(p)}}$, then the optimal maps T_2, \dots, T_P in Eq. (4) can be equivalently expressed using $P - 1$ permutations $\sigma_2, \dots, \sigma_P$ as

$$T_p(\mathbf{x}_i^{(1)}) = \mathbf{x}_{\sigma_p(i)}^{(p)} \quad \forall \mathbf{x}_i^{(1)} \in \text{Supp}(\mu_1). \quad (8)$$

This translates the problem from an optimization procedure on the space of continuous maps to on a discrete set of permutations. The discrete nature of the problem will allow us to derive a simple closed-form formula in 1D.

1D Multi-Marginal Monge–Wasserstein We now propose a closed-form formula for Eq. (4) in \mathbb{R} .

Proposition 2. *If $\mu_1, \dots, \mu_P \in \mathcal{M}^N(\mathbb{R})$, where $\mu_p =$*

$$\begin{aligned} \frac{1}{N} \sum_{i=1}^N \delta_{\tilde{x}_i^{(p)}}, \text{ with } \tilde{x}_1^{(p)} \leq \dots \leq \tilde{x}_N^{(p)}, \text{ for } p = 1, \dots, P, \\ \mathcal{MW}_2^2(\mu_1, \dots, \mu_P) = \frac{1}{N} \sum_{i,p=1}^{N,P} \beta_p \left| \tilde{x}_i^{(p)} - \sum_{j=1}^P \beta_j \tilde{x}_i^{(j)} \right|^2. \quad (9) \end{aligned}$$

Proof in Appendix A. \square

Prop. 2 states that the optimal discrete Monge maps consist of permutations that sort individual measures. Eq. (9) can be computed in $O(PN \log N)$ time. We thus have a linear complexity in the number of measures P , and an $O(N \log N)$ complexity in the number of samples per measure N .

3.2. Extending to Higher Dimensions Through Slicing

Based on the closed-form formula for the one-dimensional case in Eq. (9), we now derive a higher-dimensional extension ($d > 1$) that retains the same computational complexity with respect to N and P through the slicing approach described in Section 2.3. We define the sliced multi-marginal Wasserstein distance $\mathcal{SMW}_2^2(\mu_1, \dots, \mu_P)$ as

$$\mathcal{SMW}_2^2 = \frac{1}{\text{Vol}(S_{d-1})} \int_{S_{d-1}} \mathcal{MW}_2^2(M_{\theta \#} \mu_1, \dots, M_{\theta \#} \mu_P) d\theta \quad (10)$$

where S_{d-1} is the d -dimensional hypersphere and $M_{\theta}(x) = \langle x, \theta \rangle$. This integral can be seen as an expectation with respect to the uniform distribution on S_{d-1} . We can thus evaluate Eq. (10) by Monte-Carlo estimation, such that

$$\mathcal{SMW}_2^2 = \frac{1}{K} \sum_{k=1}^K \mathcal{MW}_2^2(M_{\theta_k \#} \mu_1, \dots, M_{\theta_k \#} \mu_P), \quad (11)$$

where $\theta_k \sim \mathcal{U}(S_{d-1})$ chooses the direction of projection uniformly at random. The overall computational complexity of Eq. (11) is $O(KPN \log N)$. Computing the sliced distance amounts to projecting, sorting individual measures, and averaging the computation of the 1D distances.

3.3. Properties

We analyze the generalized metric properties (Bento and Mi, 2020) of the one dimensional multi-marginal Monge-Wasserstein in Prop. 4 and sliced multi-marginal Monge-Wasserstein for higher dimensions in Prop. 5.

Definition 3. Assume $\mu_p \in \mathcal{M}^N(\mathcal{X})$, where $p = 1, \dots, P$, and let $D : \mathcal{M}^N(\mathcal{X}) \times \dots \times \mathcal{M}^N(\mathcal{X}) \rightarrow \mathbb{R}$. Then, D is a generalized metric if the following properties hold:

1. $D(\mu_1, \dots, \mu_P) \geq 0$
2. $D(\mu_1, \dots, \mu_P) = 0 \Leftrightarrow \mu_1 = \dots = \mu_P$
3. $D(\mu_1, \dots, \mu_P) = D(\mu_{\sigma(1)}, \dots, \mu_{\sigma(P)}), \forall \sigma \in \mathbb{S}_P$

$$\begin{aligned} 4. \quad & \forall \mu_{P+1} \in \mathcal{M}^N(\mathcal{X}) : D(\mu_1, \dots, \mu_P) \\ & \leq \sum_{p=1}^P D(\mu_1, \dots, \mu_{p-1}, \mu_{p+1}, \dots, \mu_{P+1}) \end{aligned}$$

Proposition 4. If $\beta_p = \frac{1}{P}$, then \mathcal{MW} is a generalized metric on $\mathcal{M}^N(\mathbb{R})$.

We conclude from Proposition 4 that \mathcal{MW} is a generalized metric on $\mathcal{M}^N(\mathbb{R})$ under the assumption of uniform weights β in the multi-marginal cost function.

We now study generalized metric properties of \mathcal{SMW} on the space of uniform measures with N atoms living on $\mathbb{R}^d, d \geq 1$, i.e. $\mathcal{M}^N(\mathbb{R}^d)$.

Proposition 5. If $\beta_p = \frac{1}{P}$, then \mathcal{SMW} is a generalized metric on $\mathcal{M}^N(\mathbb{R}^d)$

Proof of Propositions 4 and 5. In Appendix B. \square

Proposition 5 states that metric properties of \mathcal{MW} on the space of one-dimensional measures directly extend to higher dimensions through slicing. \mathcal{SMW} is thus a generalized metric on $\mathcal{M}^N(\mathbb{R}^d)$ for uniform β .

4. SMW as a Loss Function

We now discuss potential use cases for which the sliced multi-marginal distance can be used as a loss function.

4.1. Barycentric Averaging

The goal of barycentric averaging is to compute a mean of measures μ_1, \dots, μ_P . Using the sliced multi-marginal distance, this can be formulated as

$$\mu^* = \arg \min_{\mu \in \mathcal{M}^N(\mathbb{R}^d)} \mathcal{SMW}_2^2(\mu, \mu_1, \dots, \mu_P). \quad (12)$$

Intuitively, we aim to find a measure μ^* that is close to all other measures μ_1, \dots, μ_P , where the ‘‘closeness’’ is defined using the sliced multi-marginal distance, \mathcal{SMW}_2^2 . This is directly connected to the barycentric objective Eq. (3), which also aims at finding a measure that is close to all other measures.

Eq. (12) can be solved either by parameterizing a discrete measure $\mu = \frac{1}{N} \sum_{i=1}^N \delta_{\mathbf{x}_i}$ and optimizing locations \mathbf{x}_i , or by parameterizing a generative model $\mu = \mathbb{P}_\theta = G_\theta \# \rho$, where $\rho \in \mathcal{M}(\mathcal{Z})$ and $G_\theta : \mathcal{Z} \rightarrow \mathcal{X}$ is a parametric functional (P_θ is typically accessible through samples only) (Cohen et al., 2020).

In the following proposition, we show a connection between Eq. (3) and Eq. (12) on $\mathcal{M}^N(\mathbb{R}^d)$.

Proposition 6. If $\mu_1, \dots, \mu_P \in \mathcal{M}^N(\mathbb{R}^d)$, $D = \mathcal{SW}_2^2$, and barycentric weights are uniform, then

$$\arg \min_{\mu \in \mathcal{M}^N(\mathbb{R}^d)} \mathcal{SMW}_2^2(\mu, \mu_1, \dots, \mu_P) = \arg \min_{\mu \in \mathcal{M}^N(\mathbb{R}^d)} \mathcal{F}(\mu), \quad (13)$$

where $\mathcal{F}(\mu)$ is defined in (3). Proof in Appendix A.

This means that under the assumption of uniform barycentric weights, minimizing the sliced multi-marginal Wasserstein with respect to an additional optimized variable is equivalent to minimizing the barycentric objective. The barycenter can thus be computed through this alternative objective.

4.2. Multi-Task Regularization

Framework We consider optimizing a multi-task loss

$$\arg \min_{\nu_1, \dots, \nu_P} \sum_{p=1}^P \mathcal{L}(\mu_p, \nu_p) + \gamma \mathcal{R}(\nu_1, \dots, \nu_P), \quad (14)$$

where \mathcal{L} denotes the pairwise loss functions that are regularized by a multi-task regularizer \mathcal{R} . Usually, γ controls the amount of regularization. Intuitively, the pairwise loss \mathcal{L} aims to find good estimators ν_p of μ_p , for $p = 1, \dots, P$, while the regularizer \mathcal{R} enforces learned models ν_p s to be close. In contexts where individual tasks share structure, this can be helpful for sharing knowledge across tasks. [Janati et al. \(2019\)](#) consider this framework for multi-task regression. The regularizer \mathcal{R} is the barycentric objective in Eq. (3), hence an extra optimization variable μ (the barycenter) is added. \mathcal{R} is computed through solving an optimization problem on the space of measures, which is typically challenging and does not scale well with dimensions. Typical barycentric approaches have been constrained to $\mathbb{R}^{\leq 3}$. By contrast, we use our sliced multi-marginal distance (10) as the regularizer \mathcal{R} , which can be estimated by Monte-Carlo. It does not involve solving any extra optimization problem unlike [Janati et al. \(2019\)](#), which ensures efficiency.

Multi-Task Density Estimation We consider the problem of density estimation. Each task consists of finding a measure ν_p that is close to a measure μ_p under a pairwise metric \mathcal{L} (e.g., (Sliced) Wasserstein/Gromov-Wasserstein). For instance, we consider the optimization problem

$$\arg \min_{\nu_1, \dots, \nu_P} \sum_{p=1}^P \mathcal{SW}_2^2(\mu_p, \nu_p) + \gamma \mathcal{SMW}_2^2(\nu_1, \dots, \nu_P). \quad (15)$$

We do not require both measures to have the same support size so that, for instance, ν_p can have fewer/more support points than μ_p (in which case training needs to be done by sampling batches of identical size from both due to the same-size constraint of sliced distances). If measures share some inherent structure, regularization can be positively

impactful as it enables sharing structural knowledge across tasks, which is important if, e.g., the number of samples of μ_p s is small so it is hard to estimate well the inherent structure of the measures ([Janati et al., 2019](#)).

Multi-Task Reinforcement Learning We now discuss the application of our sliced multi-marginal distance as a regularizer in a multi-task reinforcement learning (RL) context. In our setting, there are P agents (without parameter sharing) living in different Markov decision processes $\mathcal{M}_p = (\mathcal{S}_p, \mathcal{A}_p, T_p, R_p)$, where \mathcal{S}_p is the state space, \mathcal{A}_p is the action space, and $T_p(\mathbf{x}_t^{(p)}, \mathbf{a}_t^{(p)})$ is the transition model (either stochastic or deterministic). The reward function R_p allows for sharing knowledge across tasks. It takes as input the current state $\mathbf{x}_t^{(p)}$ of the p^{th} agent and the states of all other agents at any time in the episode which we refer to as \mathbf{X} . The multi-task reward function R_p of the p^{th} agent at the t^{th} time-step is set to

$$R_p(\mathbf{x}_t^{(p)}) = r_p(\mathbf{x}_t^{(p)}) + \gamma f(r_{t,p}(\mathbf{x}_t^{(p)}, \mathbf{X})), \quad (16)$$

where $r_p(\mathbf{x}_t^{(p)})$ is the canonical reward of the p^{th} environment and $r_{t,p}(\mathbf{x}_t^{(p)}, \mathbf{X})$ is a multi-task reward arising from the \mathcal{SMW} objective. Also, $f : \mathbb{R} \rightarrow \mathbb{R}$ is a scaling function, and γ controls the impact of shared structure. In particular,

$$r_{t,p}(\mathbf{x}_t^{(p)}, \mathbf{X}) = \frac{1}{PK} \sum_{k=1}^K \left| \langle \mathbf{x}_t^{(p)} - \frac{1}{P} \sum_{j=1}^P \mathbf{x}_{\eta_{p,j,k}(t)}^{(j)}, \boldsymbol{\theta}_k \rangle \right|^2,$$

where $\eta_{p,j,k}$ returns the index of the atom in μ_j that is aligned with $\mathbf{x}_t^{(p)}$ after projecting on (Monte-Carlo-sampled) $\boldsymbol{\theta}_k$ s and sorting all projected states. Intuitively, the individual environmental reward r_p provides task-specific information, whilst the multi-task reward $r_{t,p}$ aims at enforcing agents' policies $\pi_p : \mathcal{S}_p \rightarrow \mathcal{A}_p$ to generate rollouts sharing an inherent structure. We maximize the objective

$$\mathcal{J}^\pi(\mathbf{X}) = \mathbb{E}_\pi \left[\sum_{p=1}^P \sum_{t=1}^T R_p(\mathbf{x}_t^{(p)}) \right] \quad (17)$$

with respect to the parameters of policies π_p , $p = 1, \dots, P$, where T is the horizon, P is the number of agents, and \mathbf{X} are state trajectories generated under policies π_1, \dots, π_P . We note that if $f(y) = -y$ in (16), then $\mathcal{J}^\pi(\mathbf{X})$ equals

$$\mathbb{E}_\pi \left[\sum_{p=1}^P \sum_{t=1}^T r_p(\mathbf{x}_t^{(p)}) - \gamma \mathcal{SMW}^2(\mu_1, \dots, \mu_P) \right], \quad (18)$$

where $\mu_p = \frac{1}{T} \sum_{t=1}^T \delta_{\mathbf{x}_t^{(p)}}$. Inspired by [Dadashi et al. \(2020\)](#) (similar approach in the single agent case), we also propose setting $f(y) = e^{-5y}$. We train individual agents

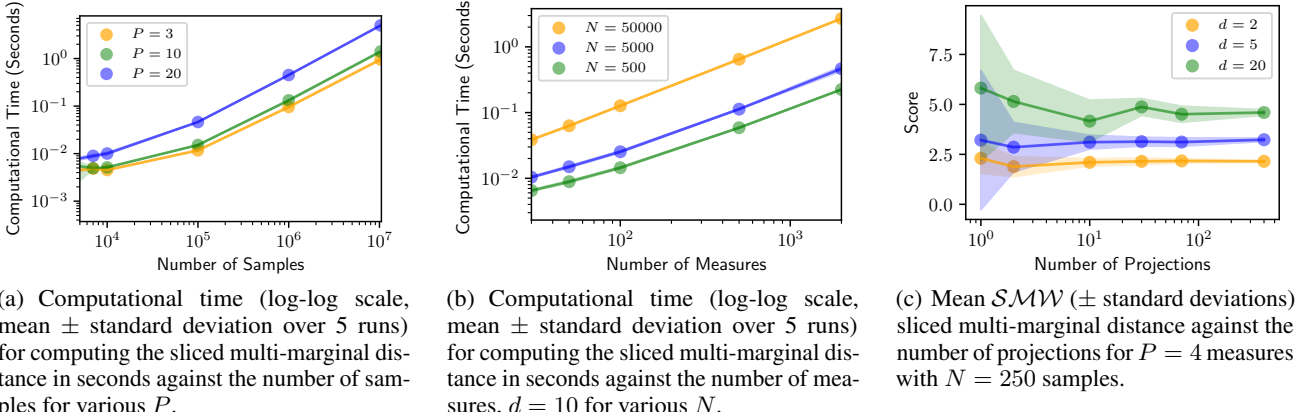


Figure 2. Properties of the sliced multi-marginal distance. (a) computational time as a function of the number of samples; (b) computational time as a function of the number of measures; (c) accuracy as a function of the number of projections

via alternation by optimizing Eq. (17) using Q -learning with function approximation with the reward structure of Eq. (16). This approach can be applied both in deterministic/stochastic settings, and a discount factor can be included.

5. Experiments

We analyze the computational costs inherent to the computation of the distance proposed in Section 3, and the impact of the number of projections on its estimation. We then analyze the properties of the proposed distance in downstream tasks including barycentric averaging and multi-task density estimation and reinforcement learning.

5.1. Analysis

Number of Samples (N). We study the impact of the number of samples on the computational time to compute the sliced multi-marginal distance in Eq. (10). In particular, we compute \mathcal{SMW} between $P = 3, 10, 20$ measures in \mathbb{R}^{10} , $\mu_p \sim \mathcal{N}(\mathbf{m}_p, \sigma^2 \mathbf{I})$, where $p = 1, \dots, P$. Figure 2(a) shows the $O(N \log N)$ scaling of \mathcal{SMW} . It enabled scaling to computing the multi-marginal distance between multiple measures (20) with over 10^7 samples (while previous approaches were constrained to $P < 5$ and $N < 10^3$).

Number of Measures (P). We now verify scalings with respect to the number of measures P . Figure 2(b) shows the time required to compute \mathcal{SMW} against the number of measures (for $N = 500, 5000, 50000$). We empirically observe the expected linear scaling of \mathcal{SMW} .

Number of Projections (K). We now discuss the impact of the number of projections on the estimation of \mathcal{SMW} for various numbers of dimensions ($d = 2, 5, 20$). We set $N = 250$, and $P = 5$. As Monte-Carlo estimation

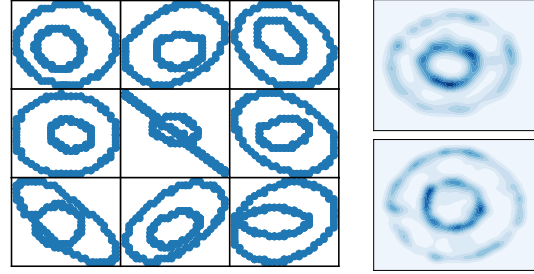


Figure 3. Averaging of 25 nested ellipses (including the ones on the left) using the \mathcal{SMW} objective (top right), and the barycentric objective Eq. (3) with $D = \mathcal{SW}^2$ (bottom right).

is performed to estimate \mathcal{SMW} . Figure 2(c) shows the expected variance shrinkage as the number of projection grows, while the estimated mean converges to \mathcal{SMW} (with rate $O(\frac{1}{\sqrt{K}})$ with constants depending on the dimension).

5.2. Computing Barycenters of Measures

We apply the proposed sliced multi-marginal distance to barycentric averaging. We investigate whether the proposed approach Eq. (12) leads to solutions with properties analogous to those of barycenters solving Eq. (3) with $D = \mathcal{SW}^2$ in a proof-of-concept experiment.

We consider a dataset of $P = 25$ nested ellipses, reproducing the example of Cuturi and Doucet (2014); Luise et al. (2019). We follow the approach by Cohen et al. (2020) for estimating barycenters by parametrizing a generative model $\mu_\theta = G_\theta \# \rho$ and training via stochastic gradient descent on the multi-marginal objective. Figure 3 shows that the solution obtained using \mathcal{SMW} is very close to the one obtained using the barycentric objective Eq. (3). Using sliced multi-marginal distances is thus a competitive alternative to the

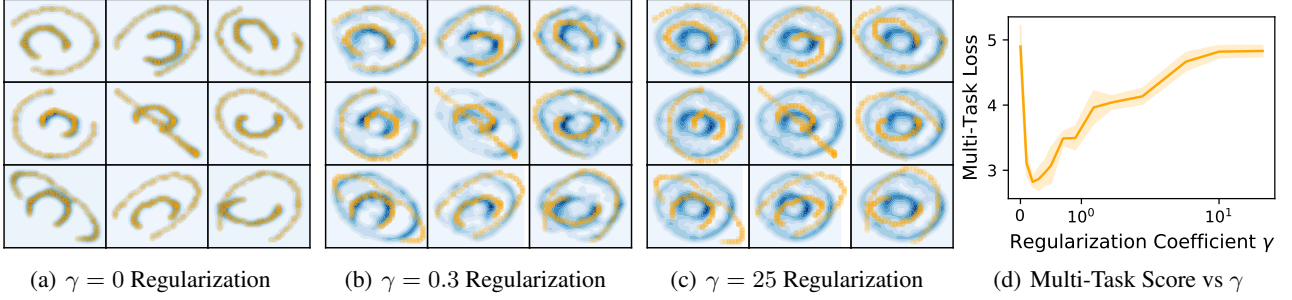


Figure 4. Multi-task density estimation experiment described in Section 4.2, and applied on corrupted versions of measures in Figure 3 (plotted in orange), using \mathcal{SW} as pairwise loss \mathcal{L} and \mathcal{SMW} as regularizer \mathcal{R} . Learned models are plotted in blue. We use $\gamma = 0$ in 4(a), $\gamma = 0.3$ in 4(b), $\gamma = 25$ in 4(c). In Figure 4(d), we also plot the multi-task loss against the regularization coefficient γ . As γ grows, the multi-task loss decreases as knowledge is shared across tasks. It then increases as solutions become too uniform.

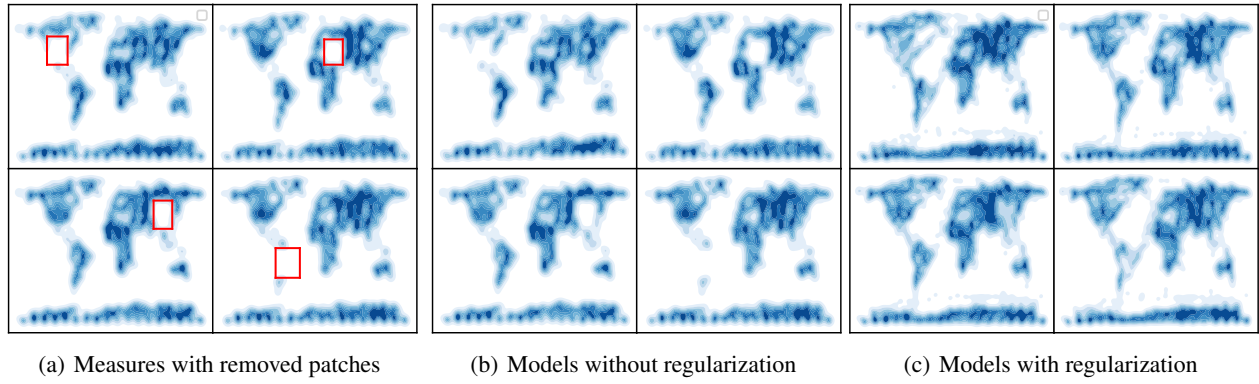


Figure 5. Multi-task density estimation experiment applied to earth data. In particular, patches are moved from different areas on the globe in the different measures in (a). We use \mathcal{SW} as pairwise loss \mathcal{L} and \mathcal{SMW} as regularizer \mathcal{R} . We use $\gamma = 0$ in (b), $\gamma = 0.5$ in (c). Regularization allows sharing the common structure across tasks and as a result ‘fill the holes’ across tasks.

barycentric objective for computing averages of probability measures, with no added computational costs.

5.3. Multi-Task Density Estimation

We consider the multi-task density estimation setting of Section 4.2. Each of the $P = 20$ density estimation tasks consists of a nested ellipse with corrupted samples. In particular, random parts of the individual ellipses have been removed from each ellipse. Using the multi-task regularization allows for sharing knowledge of the structure of the target tasks across problems. Figures 4(a)–4(c) show the models obtained by multi-task training with regularization coefficients $\gamma = 0, 0.3, 25$. When $\gamma = 0$, learned measures ν_1, \dots, ν_P collapse to the corrupted measures μ_1, \dots, μ_P . For $\gamma = 0.3$, knowledge of the inherent nested ellipse structure is shared across tasks, which leads to solutions that have such structure, but that still preserve the task-specific orientations and ellipse width/heights, while for $\gamma = 25$, solutions are identical. They collapse to a measure that is similar to the barycenter of all tasks (see Figure 3). As

γ grows, only the \mathcal{SMW} objective has weight, which enforces solutions to be close to each other.

In Figure 4(d), we plot the multi-task score ($\sum_{p=1}^P \mathcal{SW}(\mu_p^{uncorrupt}, \nu_p)$) against the regularization coefficient where $\mu_p^{uncorrupt}$ s are uncorrupted nested ellipses (see Figure 4). The loss decreases until $\gamma \approx 0.3$ as the shared knowledge leads to improvements in marginal solutions (see Figures 4(a) to 4(c)). The score worsens as solutions become uniform. We thus showed qualitatively and quantitatively that multi-task regularization can lead to better-informed solutions in this corrupted-data setting.

In Figure 5, we apply a similar pipeline to earth imagery data. We create multiple ($P = 10$) versions of the uncorrupted earth visualization by applying patches at different locations across tasks (Figure 5(a)), and illustrate 4 of such tasks for the sake of visualization. Without regularization (Figure 5(b)), holes are present in the models as expected. We then apply \mathcal{SMW} as regularizer in 5(c) (as in the ellipse experiment), and observe that this allows for sharing knowledge on the common structure in the individual tasks and

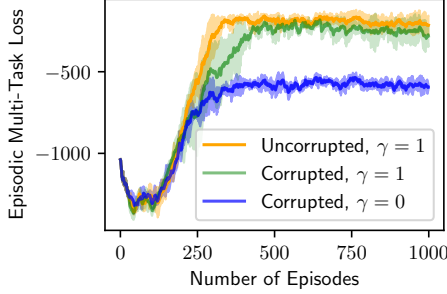


Figure 6. Multi-task ($P = 5$) RL training of agents on pendulum tasks with different dynamics. In the corrupted experiment (blue, green), 2/5 agents have corrupted rewards. Without regularization, these agents do not solve their respective tasks (blue). By contrast, with regularization, all agents learn sensible policies (green), en par with agents trained without corrupted rewards (orange).

hence learn models without patches, i.e., ‘filling the holes’.

5.4. Multi-task Reinforcement Learning

We finally consider a multi-task RL application in the setting of Section 4.2. In particular, we consider $P = 5$ pendulum tasks with different dynamics (gravities $g = 8, 9, 10, 11, 12$). Also, 2 out of 5 agents’ do not receive any reward, hence can not learn without knowledge sharing via the regularized reward function. We consider agents trained with and without \mathcal{SMW} -based regularization. Training is performed using Q-learning with function approximation on state observations (position and velocity), and using (multi-task) rewards defined in Section 4.2. We do not include discounting as it is not necessary to train in this finite-horizon problem (Bertsekas, 2005; Deisenroth and Rasmussen, 2011).

Training without regularization ($\gamma = 0$, blue curve) leads to suboptimal learning because the two agents without canonical rewards do not learn to solve their respective tasks as they get no reward. By contrast, if $\gamma = 1$, all agents (even those with no environmental reward) solve their respective tasks (green) as well (albeit slower) as if all agents were receiving environmental rewards (orange). The regularization-based rewards enforce the state trajectories of all agents to be close, and hence agents without environmental rewards learn to ‘follow’ the agents trained with canonical rewards.

6. Discussion

Similar to classical \mathcal{MW} variants, \mathcal{SMW} is geometrically motivated and metric properties (holding for specific cost functions) are preserved (under the studied cost function). By contrast with previous methods, its computation scales to a large number of measures with a massive number of atoms. These other methods do not scale because they rely on the Kantorovich formulation, which requires either solving a

linear program with N^P variables resulting in an $O(N^{3P})$ complexity, or leveraging the multi-marginal generalization of Sinkhorn’s algorithm which has $O(N^P)$ complexity per iteration. We consider the Monge problem, which allows us to derive a simple closed-form formula in the 1D case and which scales to higher dimensions via slicing.

The massive scalability of our approach comes at the price of not being able to recover a transport plan or transport maps. This is because averaging maps/plans of high-dimensional measures projected on \mathbb{R} is not meaningful, and is a common limitation of sliced OT Vayer et al. (2019); Kolouri et al. (2019); Deshpande et al. (2019b). Still, the amount of applications of evaluating scalably a multi-marginal distance is extensive as demonstrated in the experiments section.

The derivation of the closed-form formula in 1D holds specifically for the cost structure of Agueh and Carlier (2011). Such a cost makes sense in settings where it is desirable to share structure across tasks by enforcing that the learned models should be geometrically similar (e.g. in the corrupted multi-task RL/density estimation settings studied in experiments where tasks share geometric structure).

Our approach can naturally be combined with more general choices of slicing approaches, notably the nonlinear ones in Kolouri et al. (2019), and orthogonal ones in Rowland et al. (2019). The distance can be made rotationally invariant via the trick in Vayer et al. (2019), consisting of optimizing over orthogonal projections on the Stiefel manifold, and allowing to deal with spaces of different dimensions.

7. Conclusion

We proposed a massively scalable multi-marginal optimal transport distance. To achieve this, we first derive a closed-form formula for multi-marginal Monge–Wasserstein transport in the one-dimensional case, which can be computed with complexity that grows linearly in the number of marginals and $O(N \log N)$ with respect to the number of samples for \mathcal{MW} . This is in stark contrast to complexities of previous works. We then extend this distance to higher dimensions through slicing, which allows for defining a tractable multi-marginal distance in arbitrary dimensions, while retaining the favorable complexity of the one-dimensional case. We proved that \mathcal{MW} and \mathcal{SMW} are generalized metrics on the spaces of study, respectively $\mathcal{M}^N(\mathbb{R})$ and $\mathcal{M}^N(\mathbb{R}^d)$ for uniform β . We demonstrated the use \mathcal{SMW} as alternative barycentric objective for measure averaging, and as regularizer in multi-task settings, in particular in density estimation and multi-task RL, on both synthetic and real data. In contrast with previously proposed barycentric regularization methods, we do not need to estimate a barycenter jointly with the task-specific variables. The regularizer is instead estimated by Monte-Carlo.

Acknowledgments

SC was supported by the Engineering and Physical Sciences Research Council (grant number EP/S021566/1).

References

M. Aguech and G. Carlier. Barycenters in the Wasserstein space. *SIAM Journal on Mathematical Analysis*, 2011.

J. M. Altschuler and E. Boix-Adserà. Polynomial-time algorithms for multimarginal optimal transport problems with structure. *arXiv:2008.03006*, 2020.

J.-D. Benamou, G. Carlier, M. Cuturi, L. Nenna, and G. Peyré. Iterative Bregman projections for regularized transportation problems. *SIAM Journal on Scientific Computing*, 2014.

J.-D. Benamou, G. Carlier, and L. Nenna. A numerical method to solve multi-marginal optimal transport problems with Coulomb cost. In *Splitting Methods in Communication, Imaging, Science, and Engineering*. Springer, 2016.

J. Bento and L. Mi. Multi-marginal optimal transport defines a generalized metric. *arXiv:2001.11114*, 2020.

D. P. Bertsekas. *Dynamic Programming and Optimal Control*, volume I. Athena Scientific, Belmont, MA, USA, 3rd edition, 2005.

N. Bonneel and H. Pfister. Sliced Wasserstein barycenter of multiple densities. *Harvard Technical Report*, 2013.

N. Bonneel, J. Rabin, G. Peyré, and H. Pfister. Sliced and Radon Wasserstein Barycenters of Measures. *Journal of Mathematical Imaging and Vision*, 2015.

C. Bunne, D. Alvarez-Melis, A. Krause, and S. Jegelka. Learning generative models across incomparable spaces. In *ICML*, 2019.

J. Cao, L. Mo, Y. Zhang, K. Jia, C. Shen, and M. Tan. Multi-marginal Wasserstein GAN. In *NeurIPS*, 2019.

S. Cohen, M. Arbel, and M. P. Deisenroth. Estimating barycenters of measures in high dimensions. *arXiv:2007.07105*, 2020.

M. Cuturi. Sinkhorn distances: Lightspeed computation of optimal transport. In *NeurIPS*, 2013.

M. Cuturi and A. Doucet. Fast computation of Wasserstein barycenters. In *ICML*, 2014.

R. Dadashi, L. Hussenot, M. Geist, and O. Pietquin. Primal Wasserstein imitation learning. *arXiv:2006.04678*, 2020.

M. P. Deisenroth and C. E. Rasmussen. Pilco: A model-based and data-efficient approach to policy search. In *ICML*, 2011.

I. Deshpande, Y.-T. Hu, R. Sun, A. Pyrros, N. Siddiqui, S. Koyejo, Z. Zhao, D. Forsyth, and A. G. Schwing. Max-sliced Wasserstein distance and its use for GANs. In *CVPR*, 2019a.

I. Deshpande, Y.-T. Hu, R. Sun, A. Pyrros, N. Siddiqui, S. Koyejo, Z. Zhao, D. A. Forsyth, and A. G. Schwing. Max-sliced Wasserstein distance and its use for GANs. *CoRR*, 2019b.

W. Gangbo and A. Święch. Optimal maps for the multidimensional Monge-Kantorovich problem. *Communications on Pure and Applied Mathematics*, 1998.

A. Genevay, G. Peyré, and M. Cuturi. Learning generative models with Sinkhorn divergences. In *AISTATS*, 2018.

I. Haasler, A. Ringh, Y. Chen, and J. Karlsson. Multi-marginal optimal transport and Schrödinger bridges on trees. *arXiv:2004.06909*, 2020.

G. Hardy, K. M. R. Collection, J. Littlewood, G. Pólya, G. Pólya, and D. Littlewood. *Inequalities*. Cambridge University Press, 1952.

H. Janati, M. Cuturi, and A. Gramfort. Wasserstein regularization for sparse multi-task regression. In *AISTATS*, 2019.

L. V. Kantorovich. On the translocation of masses. *Journal of Mathematical Sciences*, 1958.

S. Kolouri, C. E. Martin, and G. K. Rohde. Sliced-Wasserstein autoencoder: An embarrassingly simple generative model. *arXiv:1804.01947*, 2018.

S. Kolouri, K. Nadjahi, U. Simsekli, R. Badeau, and G. Rohde. Generalized sliced Wasserstein distances. In *NeurIPS*, 2019.

T. Lin, N. Ho, M. Cuturi, and M. I. Jordan. On the complexity of approximating multimarginal optimal transport. *arXiv:1910.00152*, 2019.

G. Luise, S. Salzo, M. Pontil, and C. Ciliberto. Sinkhorn barycenters with free support via Frank-Wolfe algorithm. In *NeurIPS*, 2019.

G. Monge. Mémoire sur la théorie des déblais et des remblais. In *Histoire de l'Académie Royale des Sciences de Paris*. 1781.

F. Mémoli. Gromov-Wasserstein distances and the metric approach to object matching. *Foundations of Computational Mathematics*, 2011.

K. Nadjahi, A. Durmus, L. Chizat, S. Kolouri, S. Shahrami-
pour, and U. Simsekli. Statistical and topological proper-
ties of sliced probability divergences. *arXiv:2003.05783*,
2020.

G. Peyré and M. Cuturi. Computational optimal transport.
Foundations and Trends in Machine Learning, 2019.

G. Peyré, M. Cuturi, and J. Solomon. Gromov-Wasserstein
averaging of kernel and distance matrices. In *ICML*, 2016.

M. Rowland, J. Hron, Y. Tang, K. Choromanski, T. Sarlos,
and A. Weller. Orthogonal estimation of Wasserstein
distances. In *AISTATS*, 2019.

F. Santambrogio. *Optimal Transport for Applied Mathe-
maticians*. Springer, 2015.

N. Tupitsa, P. Dvurechensky, A. Gasnikov, and C. A. Uribe.
Multimarginal optimal transport by accelerated alternat-
ing minimization. *Transport*, 2020.

T. Vayer, R. Flamary, N. Courty, R. Tavenard, and L. Chapel.
Sliced Gromov-Wasserstein. In *NeurIPS*. 2019.

C. Villani. *Optimal Transport: Old and New*. Springer
Science & Business Media, 2008.

H. Xu, D. Luo, and L. Carin. Scalable Gromov-Wasserstein
learning for graph partitioning and matching. In *NeurIPS*.
2019a.

H. Xu, D. Luo, H. Zha, and L. C. Duke. Gromov-
Wasserstein learning for graph matching and node em-
bedding. In *ICML*, 2019b.

A. Closed-Form Formulas

A.1. Proof of multi-marginal Wasserstein in 1D

We aim to prove the following proposition:

Proposition 7. *Let $\mu_1, \dots, \mu_P \in \mathcal{M}^N(\mathbb{R})$ be P marginals, $\beta \in \Delta_P$ where Δ_P is the P -simplex and let us assume atoms of μ_p 's are sorted, i.e. $\tilde{x}_1^{(j)} \leq \dots \leq \tilde{x}_N^{(j)} \forall j = 1, \dots, P$. Then,*

$$\mathcal{MW}_2^2(\mu_1, \dots, \mu_P) = \frac{1}{N} \sum_{n=1}^N \sum_{p=1}^P \beta_p |\tilde{x}_n^{(p)} - \sum_{j=1}^P \beta_j \tilde{x}_n^{(j)}|^2 \quad (19)$$

We will use the following result, noting that we define \mathbb{S}_N as the set of permutations of order N :

Proposition 8. *For any permutations $\sigma_p, \sigma_j \in \mathbb{S}_N$, and if $\tilde{x}_1^{(k)} \leq \dots \leq \tilde{x}_N^{(k)} \forall k = 1, \dots, P$ the following holds:*

$$\sum_{n=1}^N \tilde{x}_{\sigma_p(n)}^{(p)} \tilde{x}_{\sigma_j(n)}^{(j)} \leq \sum_{n=1}^N \tilde{x}_n^{(p)} \tilde{x}_n^{(j)} \quad (20)$$

Proof. The rearrangement inequality (Hardy et al., 1952) shows that $\forall \sigma \in \mathbb{S}_N$,

$$\sum_{n=1}^N \tilde{x}_n^{(p)} \tilde{x}_{\sigma(n)}^{(j)} \leq \sum_{n=1}^N \tilde{x}_n^{(p)} \tilde{x}_n^{(j)} \quad (21)$$

Let $\sigma' \in \mathbb{S}_N$ be the permutation such that $\sigma_p \circ \sigma' = \sigma_j$. Then:

$$\sum_{n=1}^N \tilde{x}_n^{(p)} \tilde{x}_{\sigma'(n)}^{(j)} \leq \sum_{n=1}^N \tilde{x}_n^{(p)} \tilde{x}_n^{(j)} \quad (22)$$

$$\Rightarrow \sum_{n=1}^N \tilde{x}_{\sigma_p(n)}^{(p)} \tilde{x}_{\sigma_j(n)}^{(j)} = \sum_{n=1}^N \tilde{x}_{\sigma_p(n)}^{(p)} \tilde{x}_{\sigma_p(\sigma'(n))}^{(j)} = \sum_{n=1}^N \tilde{x}_n^{(p)} \tilde{x}_{\sigma'(n)}^{(j)} \leq \sum_{n=1}^N \tilde{x}_n^{(p)} \tilde{x}_n^{(j)}, \quad (23)$$

noting that Eq. (22) holds because of Eq. (21), and the second equality in (23) holds by the invariance of sums under permutations (here σ_p). \square

We now proceed to proving the result enabling us to compute the multi-marginal Wasserstein in closed-form.

Proof of Proposition 7. $\mu_1, \dots, \mu_P \in \mathcal{M}^N(\mathbb{R})$ holds, thus we can use Proposition 1 to rewrite the objective in Proposition 7 as follows:

$$\min_{(T_2, \dots, T_P) \in \mathcal{T}(\mu_1, \dots, \mu_P)} \int \sum_{p=1}^P \beta_p \|T_p(x) - \sum_{j=1}^P \beta_j T_j(x)\|^2 d\mu_1(x) \quad (24)$$

$$= \min_{(T_2, \dots, T_P) \in \mathcal{T}(\mu_1, \dots, \mu_P)} \frac{1}{N} \sum_{n=1}^N \sum_{p=1}^P \beta_p \|T_p(\tilde{x}_n^{(1)}) - \sum_{j=1}^P \beta_j T_j(\tilde{x}_n^{(1)})\|^2 \quad (25)$$

$$= \min_{\sigma_2, \dots, \sigma_P \in \mathbb{S}_N | \sigma_1 = I_N} \frac{1}{N} \sum_{n=1}^N \sum_{p=1}^P \beta_p |\tilde{x}_{\sigma_p(n)}^{(p)} - \sum_{j=1}^P \beta_j \tilde{x}_{\sigma_j(n)}^{(j)}|^2 \quad (26)$$

Eq. (24) \rightarrow Eq. (25) holds because μ_1 is a discrete uniform measure with N atoms, Eq. (25) \rightarrow Eq. (26) holds because individual Monge maps are bijections $T_p(\tilde{x}_i^{(1)}) = \tilde{x}_{\sigma_p(i)}^{(p)}$. For any set of permutations $\sigma_p \in \mathbb{S}_N, p = 2, \dots, P$ (σ_1 is set to be the identity permutation I_N),

$$\frac{1}{N} \sum_{n=1}^N \sum_{p=1}^P \beta_p |\tilde{x}_{\sigma_p(n)}^{(p)} - \sum_{j=1}^P \beta_j \tilde{x}_{\sigma_j(n)}^{(j)}|^2 \quad (27)$$

$$= \frac{1}{N} \sum_{n=1}^N \sum_{p=1}^P \beta_p |\tilde{x}_n^{(p)}|^2 + \frac{1}{N} \sum_{n=1}^N \left| \sum_{j=1}^P \beta_j \tilde{x}_{\sigma_j(n)}^{(j)} \right|^2 - \frac{2}{N} \sum_{n=1}^N \sum_{p=1}^P \beta_p \tilde{x}_{\sigma_p(n)}^{(p)} \left(\sum_{j=1}^P \beta_j \tilde{x}_{\sigma_j(n)}^{(j)} \right) \quad (28)$$

$$= \frac{1}{N} \sum_{n=1}^N \sum_{p=1}^P \beta_p |\tilde{x}_n^{(p)}|^2 - \frac{1}{N} \sum_{n=1}^N \left[\sum_{p=1}^P \beta_p \tilde{x}_{\sigma_p(n)}^{(p)} \right] \left[\sum_{j=1}^P \beta_j \tilde{x}_{\sigma_j(n)}^{(j)} \right] \quad (29)$$

$$= \frac{1}{N} \sum_{n=1}^N \sum_{p=1}^P \beta_p |\tilde{x}_n^{(p)}|^2 - \frac{1}{N} \sum_{p=1}^P \sum_{j=1}^P \beta_p \beta_j \sum_{n=1}^N \tilde{x}_{\sigma_p(n)}^{(p)} \tilde{x}_{\sigma_j(n)}^{(j)} \quad (30)$$

$$\geq \frac{1}{N} \sum_{n=1}^N \sum_{p=1}^P \beta_p |\tilde{x}_n^{(p)}|^2 - \frac{1}{N} \sum_{p=1}^P \sum_{j=1}^P \beta_p \beta_j \sum_{n=1}^N \tilde{x}_n^{(p)} \tilde{x}_n^{(j)} \quad (31)$$

$$= \frac{1}{N} \sum_{n=1}^N \sum_{p=1}^P \beta_p |\tilde{x}_n^{(p)}| - \sum_{j=1}^P \beta_j \tilde{x}_n^{(j)} \quad (32)$$

Eq. (28) because β lies in a P -simplex. The inequality Eq. (31) holds because of Proposition 8. Previous equalities follow simply by expanding the square.

This proves that the arg-minimization results in identity maps (provided that the $\tilde{x}_p^{(n)}$'s are sorted), from which we can conclude the proof. \square

A.2. Proof of Equivalence of Barycentric Objectives

We aim to prove the following proposition:

Proposition 9. *If $\mu_1, \dots, \mu_P \in \mathcal{M}^N(\mathbb{R}^d)$, $\beta_p = \frac{1}{P} \forall p = 1, \dots, P$ for the barycentric objective, $\beta_p = \frac{1}{P+1} \forall p = 1, \dots, P+1$ for the \mathcal{SMW}^2 objective, and $D = \mathcal{SW}_2^2$ then*

$$\arg \min_{\mu \in \mathcal{M}^N(\mathbb{R}^d)} \mathcal{SMW}_2^2(\mu, \mu_1, \dots, \mu_P) = \arg \min_{\mu \in \mathcal{M}^N(\mathbb{R}^d)} \mathcal{F}(\mu) \quad (33)$$

Proof. Firstly, the RHS can be expressed as follows:

$$\arg \min_{\mu \in \mathcal{M}^N(\mathbb{R}^d)} \mathcal{F}(\mu) \quad (34)$$

$$= \arg \min_{\mu \in \mathcal{M}^N(\mathbb{R}^d)} \frac{1}{P} \sum_{p=1}^P \mathcal{SW}_2^2(\mu_p, \mu) \quad (35)$$

$$= \arg \min_{\mathbf{x}_1, \dots, \mathbf{x}_N} \frac{1}{P} \sum_{p=1}^P \mathcal{SW}_2^2(\mu_p, \mu) \quad (36)$$

$$= \arg \min_{\mathbf{x}_1, \dots, \mathbf{x}_N} \frac{1}{NP\text{Vol}(S_{d-1})} \sum_{p=1}^P \int_{S_{d-1}} \sum_{i=1}^N |\tilde{x}_{i,\theta} - \tilde{x}_{i,\theta}^{(p)}|^2 d\theta \quad (37)$$

$$= \arg \min_{\mathbf{x}_1, \dots, \mathbf{x}_N} \sum_{p=1}^P \int_{S_{d-1}} \sum_{i=1}^N |\tilde{x}_{i,\theta} - \tilde{x}_{i,\theta}^{(p)}|^2 d\theta \quad (38)$$

Eq. (34) \rightarrow Eq. (35) is by definition. Eq. (35) \rightarrow Eq. (36) uses the fact that minimization on $\mathcal{M}^N(\mathbb{R}^d)$ is equivalent to minimization on N atoms of $\mathbf{x}_1, \dots, \mathbf{x}_N$ and the rest of the proof uses the definition

$$\mathcal{SW}_2^2(\mu_p, \mu) = \frac{1}{N\text{Vol}(S_{d-1})} \int_{S_{d-1}} \sum_{i=1}^N |\tilde{x}_{i,\theta} - \tilde{x}_{i,\theta}^{(p)}|^2 d\theta,$$

where $\tilde{x}_{i,\theta} = \text{sort}([\langle \mathbf{x}_1, \theta \rangle, \dots, \langle \mathbf{x}_N, \theta \rangle])_i$ and $\tilde{x}_{i,\theta}^{(p)} = \text{sort}([\langle \mathbf{x}_1^{(p)}, \theta \rangle, \dots, \langle \mathbf{x}_N^{(p)}, \theta \rangle])_i$.

Secondly, the LHS can be expressed as :

$$\arg \min_{\mathbf{x}_1, \dots, \mathbf{x}_N} \mathcal{SMW}_2^2(\mu, \mu_1, \dots, \mu_P) \quad (39)$$

$$= \arg \min_{\mathbf{x}_1, \dots, \mathbf{x}_N} \frac{1}{N(P+1)\text{Vol}(S_{d-1})} \int_{S_{d-1}} \sum_{i=1}^N \sum_{p=1}^{P+1} \left| \tilde{x}_{i,\theta}^{(p)} - \frac{1}{P+1} \sum_{j=1}^{P+1} \tilde{x}_{i,\theta}^{(j)} \right|^2 d\theta \quad (40)$$

$$= \arg \min_{\mathbf{x}_1, \dots, \mathbf{x}_N} \frac{1}{2N(P+1)^2\text{Vol}(S_{d-1})} \int_{S_{d-1}} \sum_{i=1}^N \sum_{p=1}^{P+1} \sum_{p'=1}^{P+1} \left| \tilde{x}_{i,\theta}^{(p)} - \tilde{x}_{i,\theta}^{(p')} \right|^2 d\theta \quad (41)$$

$$= \arg \min_{\mathbf{x}_1, \dots, \mathbf{x}_N} \frac{1}{N(P+1)^2\text{Vol}(S_{d-1})} \int_{S_{d-1}} \sum_{p=1}^P \sum_{i=1}^N \left| \tilde{x}_{i,\theta} - \tilde{x}_{i,\theta}^{(p)} \right|^2 d\theta \quad (42)$$

$$= \arg \min_{\mathbf{x}_1, \dots, \mathbf{x}_N} \sum_{p=1}^P \int_{S_{d-1}} \sum_{i=1}^N \left| \tilde{x}_{i,\theta} - \tilde{x}_{i,\theta}^{(p)} \right|^2 d\theta \quad (43)$$

Eq. (39) \rightarrow Eq. (40) uses the definition of

$$\mathcal{SMW}_2^2(\mu_1, \dots, \mu_P) = \frac{1}{\text{Vol}(S_{d-1})} \int_{S_{d-1}} \mathcal{MW}_2^2(M_{\theta_k \# \mu_1}, \dots, M_{\theta_k \# \mu_P}) d\theta. \quad (44)$$

(Santambrogio, 2015)(page 195) shows that Eq. (40) \rightarrow Eq. (41). In particular,

$$\frac{1}{2(P+1)^2} \sum_{p,p'=1}^{P+1} \left| \tilde{x}_{i,\theta}^{(p)} - \tilde{x}_{i,\theta}^{(p')} \right|^2 = \frac{1}{P+1} \sum_{p=1}^{P+1} \left| \tilde{x}_{i,\theta}^{(p)} \right|^2 - \left| \frac{1}{P+1} \sum_{p=1}^{P+1} \tilde{x}_{i,\theta}^{(p)} \right|^2 = \frac{1}{P+1} \sum_{p=1}^{P+1} \left| \tilde{x}_{i,\theta}^{(p)} - \frac{1}{P+1} \sum_{j=1}^{P+1} \tilde{x}_{i,\theta}^{(j)} \right|^2 \quad (45)$$

Eq. (41) \rightarrow Eq. (42) holds as the minimization uses only the terms where either $p = 1$ or $p' = 1$. \square

B. Generalized Metric Properties

We now study generalized metric properties of \mathcal{MW} and \mathcal{SMW} on respectively $\mathcal{M}^N(\mathbb{R})$ and $\mathcal{M}^N(\mathbb{R}^d)$.

A generalized metric $D : \mathcal{M}(\mathcal{X}) \times \dots \times \mathcal{M}(\mathcal{X}) \rightarrow \mathbb{R}^+$ satisfies the following properties (Bento and Mi, 2020):

1. $D(\mu_1, \dots, \mu_P) \geq 0 \quad \forall \mu_p \in \mathcal{M}(\mathcal{X}), p = 1, \dots, P$
2. $D(\mu_1, \dots, \mu_P) = 0 \Leftrightarrow \mu_1 = \dots = \mu_P$
3. $D(\mu_1, \dots, \mu_P) = D(\mu_{\sigma(1)}, \dots, \mu_{\sigma(P)}) \quad \forall \sigma \in \mathbb{S}_P$
4. $D(\mu_1, \dots, \mu_P) \leq \sum_{p=1}^N D(\mu_1, \dots, \mu_{p-1}, \mu_{p+1}, \dots, \mu_P, \mu_{P+1}) \quad \forall \mu_{P+1} \in \mathcal{M}(\mathcal{X}).$

B.1. Generalized Metric Properties of Multi-Marginal Transport in 1D

We now prove generalized metric properties of \mathcal{MW} on $\mathcal{M}^N(\mathbb{R})$. Thus $\mu = \frac{1}{N} \sum_{n=1}^N \delta_{x_n} \forall \mu \in \mathcal{M}^N(\mathbb{R})$. Note that throughout this section, we refer to sorted samples as $\tilde{x}_i^{(p)} : \tilde{x}_1^{(p)} \leq \dots \leq \tilde{x}_N^{(p)} \quad \forall p$, and $\beta \in \Delta_P$.

We begin by reminding the following formula for $\mu_1, \dots, \mu_P \in \mathcal{M}^N(\mathbb{R})$:

$$\mathcal{MW}_2^2(\mu_1, \dots, \mu_P) = \frac{1}{N} \sum_{i=1}^N \sum_{p=1}^P \beta_p \left| \tilde{x}_i^{(p)} - \sum_{j=1}^P \beta_j \tilde{x}_i^{(j)} \right|^2 \quad (46)$$

Proposition 10. $\mathcal{MW}(\mu_1, \dots, \mu_P) \geq 0$ for all $\mu_p \in \mathcal{M}^N(\mathbb{R})$

Proof.

$$\mathcal{MW}(\mu_1, \dots, \mu_P) = \left(\frac{1}{N} \sum_{i=1}^N \sum_{p=1}^P \beta_p |\tilde{x}_i^{(p)} - \sum_{j=1}^P \beta_j \tilde{x}_i^{(j)}|^2 \right)^{\frac{1}{2}} \geq 0 \quad (47)$$

□

Proposition 11. If $\beta_p = \frac{1}{P} \quad \forall p = 1, \dots, P$, $\mathcal{MW}(\mu_1, \dots, \mu_P) = 0 \Leftrightarrow \mu_1 = \dots = \mu_P$

Proof. We begin by proving the forward implication (\Rightarrow).

$$\mathcal{MW}(\mu_1, \dots, \mu_P) = 0 \quad (48)$$

$$\Rightarrow \left(\frac{1}{N} \sum_{i=1}^N \sum_{p=1}^P \beta_p |\tilde{x}_i^{(p)} - \sum_{j=1}^P \beta_j \tilde{x}_i^{(j)}|^2 \right)^{\frac{1}{2}} = 0 \quad (49)$$

$$\Rightarrow \frac{1}{N} \sum_{i=1}^N \sum_{p=1}^P \beta_p |\tilde{x}_i^{(p)} - \sum_{j=1}^P \beta_j \tilde{x}_i^{(j)}|^2 = 0 \quad (50)$$

$$\Rightarrow \tilde{x}_i^{(p)} - \sum_{j=1}^P \beta_j \tilde{x}_i^{(j)} = 0 \quad \forall p = 1, \dots, P, \forall i = 1, \dots, N \quad (51)$$

Now assume for contradiction that $\exists m, n : \tilde{x}_i^{(m)} \neq \tilde{x}_i^{(n)}$, then:

$$\tilde{x}_i^{(m)} = \sum_{j=1}^P \beta_j \tilde{x}_i^{(j)}, \quad \tilde{x}_i^{(n)} = \sum_{j=1}^P \beta_j \tilde{x}_i^{(j)} \quad (52)$$

$$\Leftrightarrow \tilde{x}_i^{(m)} - \tilde{x}_i^{(n)} = \sum_{j=1}^P \beta_j \tilde{x}_i^{(j)} - \sum_{j=1}^P \beta_j \tilde{x}_i^{(j)} = 0 \quad (53)$$

which is a contradiction, therefore $\tilde{x}_i^{(m)} = \tilde{x}_i^{(n)} \quad \forall i, m, n$, thus $\mu_1 = \dots = \mu_P$

We continue by proving the backward implication (\Leftarrow).

If $\mu_1 = \dots = \mu_P$, then $\tilde{x}_i^{(p)} = \tilde{x}_i^{(p')} \quad \forall i = 1, \dots, N, \forall p, p' = 1, \dots, P$ because atoms are sorted.

Therefore, $\tilde{x}_i^{(p)} - \sum_{j=1}^P \beta_j \tilde{x}_i^{(j)} = 0 \quad \forall p = 1, \dots, P, \forall i = 1, \dots, N$.

Thus

$$\mathcal{MW}(\mu_1, \dots, \mu_P) = \left(\frac{1}{N} \sum_{i=1}^N \sum_{p=1}^P \beta_p |\tilde{x}_i^{(p)} - \sum_{j=1}^P \beta_j \tilde{x}_i^{(j)}|^2 \right)^{\frac{1}{2}} = 0 \quad (54)$$

□

Proposition 12. If $\beta_p = \frac{1}{P} \quad \forall p = 1, \dots, P$, $\mathcal{MW}(\mu_1, \dots, \mu_P) = \mathcal{MW}(\mu_{\sigma(1)}, \dots, \mu_{\sigma(P)}) \quad \forall \sigma \in \mathbb{S}_N$

Proof.

$$\mathcal{MW}(\mu_1, \dots, \mu_P) = \left(\frac{1}{NP} \sum_{i=1}^N \sum_{p=1}^P |\tilde{x}_i^{(p)} - \frac{1}{P} \sum_{j=1}^P \tilde{x}_i^{(j)}|^2 \right)^{\frac{1}{2}} \quad (55)$$

$$= \left(\frac{1}{NP} \sum_{i=1}^N \sum_{p=1}^P |\tilde{x}_i^{(p)} - \frac{1}{P} \sum_{j=1}^P \tilde{x}_i^{\sigma(j)}|^2 \right)^{\frac{1}{2}} \quad (56)$$

$$= \left(\frac{1}{NP} \sum_{i=1}^N \sum_{p=1}^P |\tilde{x}_i^{\sigma(p)} - \frac{1}{P} \sum_{j=1}^P \tilde{x}_i^{\sigma(j)}|^2 \right)^{\frac{1}{2}} \quad (57)$$

$$= \mathcal{MW}(\mu_{\sigma(1)}, \dots, \mu_{\sigma(P)}) \quad (58)$$

Both equalities hold because of the invariance of the summation operator with respect to any permutation $\sigma \in \mathbb{S}_P$. □

Proposition 13. If $\beta_p = \frac{1}{P} \quad \forall p$, $\mathcal{MW}(\mu_1, \dots, \mu_P) \leq \sum_{p=1}^N \mathcal{MW}(\mu_1, \dots, \mu_{p-1}, \mu_{p+1}, \dots, \mu_P, \mu_{P+1}) \quad \forall \mu_{P+1} \in \mathcal{M}^N(\mathbb{R})$.

Proof. We begin by proving the case $P \geq 3$ Firstly, we rewrite the multi-marginal functional in the following way:

$$\mathcal{MW}^2(\mu_1, \dots, \mu_P) = \frac{1}{N} \sum_{i=1}^N \sum_{p=1}^P \beta_p \left| \tilde{x}_i^{(p)} - \sum_{j=1}^P \beta_j \tilde{x}_i^{(j)} \right|^2 \quad (59)$$

$$= \frac{1}{NP} \sum_{i=1}^N \sum_{p=1}^P \left| \tilde{x}_i^{(p)} - \frac{1}{P} \sum_{j=1}^P \tilde{x}_i^{(j)} \right|^2 \quad (60)$$

$$= \frac{1}{2NP^2} \sum_{i=1}^N \sum_{m,n=1}^P |\tilde{x}_i^{(m)} - \tilde{x}_i^{(n)}|^2 \quad (61)$$

$$= \frac{1}{2NP^2} \sum_{i=1}^N \sum_{m,n=1}^P \theta_{i,n,m}^2 \quad (62)$$

where $\theta_{i,n,m} = |\tilde{x}_i^{(m)} - \tilde{x}_i^{(n)}|$. Eq. (61) holds because of the result in Santambrogio (2015):

$$\frac{1}{2P^2} \sum_{m,n=1}^P |\tilde{x}_i^{(m)} - \tilde{x}_i^{(n)}|^2 = \frac{1}{P} \sum_{m=1}^P |\tilde{x}_i^{(m)}|^2 - \left| \frac{1}{P} \sum_{m=1}^P \tilde{x}_i^{(m)} \right|^2 = \frac{1}{P} \sum_{m=1}^P \left| \tilde{x}_i^{(m)} - \frac{1}{P} \sum_{j=1}^P \tilde{x}_i^{(j)} \right|^2 \quad (63)$$

Therefore, we have:

$$\sum_{p=1}^P \mathcal{MW}^2(\mu_1, \dots, \mu_{p-1}, \mu_{p+1}, \dots, \mu_{P+1}) = \frac{1}{2NP^2} \sum_{p=1}^P \sum_{i=1}^N \sum_{m,n \neq p}^{P+1} \theta_{i,n,m}^2 \quad (64)$$

□

We now show that $\sum_{p=1}^P \sum_{i=1}^N \sum_{m,n \neq p}^{P+1} \theta_{i,n,m}^2 \geq \sum_{i=1}^N \sum_{m,n=1}^P \theta_{i,n,m}^2$. This can be observed by noting that all $\theta_{i,m',n'}^2$ terms on the RHS appear on the LHS. Indeed, for any m', n' , $\theta_{i,n',m'}^2$ appears in the $p \neq m', n'$ summation, which always holds for some p as $P \geq 3$.

Therefore, we have shown that

$$\mathcal{MW}^2(\mu_1, \dots, \mu_P) \leq \sum_{p=1}^P \mathcal{MW}^2(\mu_1, \dots, \mu_{p-1}, \mu_{p+1}, \dots, \mu_{P+1}) \quad (65)$$

Also,

$$\mathcal{MW}^2(\mu_1, \dots, \mu_P) \leq \sum_{p=1}^P \mathcal{MW}^2(\mu_1, \dots, \mu_{p-1}, \mu_{p+1}, \dots, \mu_{P+1}) \quad (66)$$

$$\Rightarrow \mathcal{MW}(\mu_1, \dots, \mu_P) \leq \sqrt{\sum_{p=1}^P \mathcal{MW}^2(\mu_1, \dots, \mu_{p-1}, \mu_{p+1}, \dots, \mu_{P+1})} \quad (67)$$

$$\leq \sum_{p=1}^P \sqrt{\mathcal{MW}^2(\mu_1, \dots, \mu_{p-1}, \mu_{p+1}, \dots, \mu_{P+1})} \quad (68)$$

$$= \sum_{p=1}^P \mathcal{MW}(\mu_1, \dots, \mu_{p-1}, \mu_{p+1}, \dots, \mu_{P+1}) \quad (69)$$

which proves the result. The case $P = 2$ has been proved via different approaches (e.g. [Peyré and Cuturi \(2019\)](#)).

B.2. Generalized Metric properties of Sliced Multi-Marginal Transport

We remind the definition of \mathcal{SMW} on $\mathcal{M}^N(\mathbb{R}^d)$:

$$\mathcal{SMW}(\mu_1, \dots, \mu_P) = \left(\frac{1}{\text{Vol}(S_{d-1})} \int_{S_{d-1}} \mathcal{MW}^2(M_{\theta\#}\mu_1, \dots, M_{\theta\#}\mu_P) d\theta \right)^{\frac{1}{2}} \quad (70)$$

Proposition 14. $\mathcal{SMW}(\mu_1, \dots, \mu_P) \geq 0$ for all $\mu_p = \frac{1}{N} \sum_{n=1}^N \delta_{\mathbf{x}_n^{(p)}}$

Proof. Direct from the definition of the sliced distance Eq. (70). □

Proposition 15. If $\beta_p = \frac{1}{P} \quad \forall p$, $\mathcal{SMW}(\mu_1, \dots, \mu_P) = 0 \Leftrightarrow \mu_1 = \dots = \mu_P$

Proof. We begin with the forward direction (\Rightarrow).

We extend the proof of [Nadjahi et al. \(2020\)](#) to the multi-marginal case. Define α as the uniform distribution on S_{d-1} . Define 'for (α -almost-every) θ ' as $\forall \alpha\text{-a-e-}\theta$. Firstly, the following hold:

$$\mathcal{SMW}(\mu_1, \dots, \mu_P) = 0 \quad (71)$$

$$\Rightarrow \left(\frac{1}{\text{Vol}(S_{d-1})} \int_{S_{d-1}} \mathcal{MW}^2(M_{\theta\#}\mu_1, \dots, M_{\theta\#}\mu_P) d\theta \right)^{\frac{1}{2}} = 0 \quad (72)$$

$$\Rightarrow \mathcal{MW}(M_{\theta\#}\mu_1, \dots, M_{\theta\#}\mu_P) \forall \alpha\text{-a-e-}\theta \quad (73)$$

$$\Rightarrow M_{\theta\#}\mu_1 = \dots = M_{\theta\#}\mu_P \forall \alpha\text{-a-e-}\theta \quad (74)$$

Next, we define the Fourier transform of any measure μ on $\mathcal{M}^N(\mathbb{R}^s)$, $s \geq 1$ at any $\mathbf{w} \in \mathbb{R}^s$:

$$\mathcal{F}[\mu](\mathbf{w}) = \int_{\mathbb{R}^s} e^{-i\langle \mathbf{w}, \mathbf{x} \rangle} d\mu(\mathbf{x}). \quad (75)$$

Therefore, using properties of push-forwards, the following holds:

$$\mathcal{F}[M_{\theta\#}\mu](t) = \int_{\mathbb{R}} e^{-itu} dM_{\theta\#}\mu(u) = \int_{\mathbb{R}^s} e^{-it\langle \theta, \mathbf{x} \rangle} d\mu(\mathbf{x}) = \mathcal{F}[\mu](t\theta). \quad (76)$$

As $\forall \alpha\text{-a-e-}\theta$, $M_{\theta\#}\mu_1 = \dots = M_{\theta\#}\mu_P$, then $\mathcal{F}[M_{\theta\#}\mu_1] = \dots = \mathcal{F}[M_{\theta\#}\mu_P]$, which implies that $\mathcal{F}[\mu_1] = \dots = \mathcal{F}[\mu_P]$. By injectivity of the Fourier transform, we conclude that $\mu_1 = \dots = \mu_P$

We continue with the backward direction (\Leftarrow).

We thus assume $\mu_1 = \dots = \mu_P$, which implies the following:

$$\mu_1 = \dots = \mu_P \quad (77)$$

$$\Rightarrow M_{\theta\#}\mu_1 = \dots = M_{\theta\#}\mu_P \forall \alpha\text{-a-e-}\theta \quad (78)$$

$$\Rightarrow \mathcal{MW}^2(M_{\theta\#}\mu_1, \dots, M_{\theta\#}\mu_P) = 0 \forall \alpha\text{-a-e-}\theta \quad (79)$$

$$\Rightarrow \mathcal{SMW}(\mu_1, \dots, \mu_P) = \left(\frac{1}{\text{Vol}(S_{d-1})} \int_{S_{d-1}} \mathcal{MW}^2(M_{\theta\#}\mu_1, \dots, M_{\theta\#}\mu_P) d\theta \right)^{\frac{1}{2}} = 0 \quad (80)$$

□

Proposition 16. If $\beta_p = \frac{1}{P} \quad \forall p$, $\mathcal{SMW}(\mu_1, \dots, \mu_P) = \mathcal{SMW}(\mu_{\sigma(1)}, \dots, \mu_{\sigma(P)}) \forall \sigma \in \mathbb{S}_P$

Proof.

$$\mathcal{SMW}(\mu_1, \dots, \mu_P) = \left(\frac{1}{\text{Vol}(S_{d-1})} \int_{S_{d-1}} \mathcal{MW}^2(M_{\theta\#}\mu_1, \dots, M_{\theta\#}\mu_P) d\theta \right)^{\frac{1}{2}} \quad (81)$$

$$= \left(\frac{1}{\text{Vol}(S_{d-1})} \int_{S_{d-1}} \mathcal{MW}^2(M_{\theta\#}\mu_{\sigma(1)}, \dots, M_{\theta\#}\mu_{\sigma(P)}) d\theta \right)^{\frac{1}{2}} \quad (82)$$

$$= \mathcal{SMW}(\mu_{\sigma(1)}, \dots, \mu_{\sigma(P)}) \quad (83)$$

where the second inequality holds directly from Proposition 12. □

Proposition 17. If $\beta_p = \frac{1}{P} \quad \forall p$, $\mathcal{SMW}(\mu_1, \dots, \mu_P) \leq \sum_{p=1}^N \mathcal{SMW}(\mu_1, \dots, \mu_{p-1}, \mu_{p+1}, \dots, \mu_P, \mu_{P+1}) \quad \forall \mu_{P+1} \in \mathcal{M}^N(\mathbb{R}^d)$.

Proof. In the proof of Proposition 13, we showed that:

$$\mathcal{MW}^2(\mu_1, \dots, \mu_P) \leq \sum_{p=1}^P \mathcal{MW}^2(\mu_1, \dots, \mu_{p-1}, \mu_{p+1}, \dots, \mu_{P+1}). \quad (84)$$

This implies that:

$$\mathcal{SMW}^2(\mu_1, \dots, \mu_P) \quad (85)$$

$$= \frac{1}{\text{Vol}(S_{d-1})} \int_{S_{d-1}} \mathcal{MW}^2(M_{\theta\#}\mu_1, \dots, M_{\theta\#}\mu_P) d\theta \quad (86)$$

$$\leq \sum_{p=1}^P \frac{1}{\text{Vol}(S_{d-1})} \int_{S_{d-1}} \mathcal{MW}^2(M_{\theta\#}\mu_1, \dots, M_{\theta\#}\mu_{p-1}, M_{\theta\#}\mu_{p+1}, \dots, M_{\theta\#}\mu_{P+1}) d\theta \quad (87)$$

$$= \sum_{p=1}^P \mathcal{SMW}^2(\mu_1, \dots, \mu_{p-1}, \mu_{p+1}, \dots, \mu_{P+1}) \quad (88)$$

And therefore we can conclude the following:

$$\mathcal{SMW}^2(\mu_1, \dots, \mu_P) \leq \sum_{p=1}^P \mathcal{SMW}^2(\mu_1, \dots, \mu_{p-1}, \mu_{p+1}, \dots, \mu_{P+1}) \quad (89)$$

$$\Rightarrow \mathcal{SMW}(\mu_1, \dots, \mu_P) \leq \sum_{p=1}^P \mathcal{SMW}(\mu_1, \dots, \mu_{p-1}, \mu_{p+1}, \dots, \mu_{P+1}) \quad (90)$$

directly in the same way as in the proof of Proposition 13. \square

C. Extra Experimental Details

Barycentric Averaging We follow the experimental setting of Cohen et al. (2020), consisting of parametrizing a barycenter as a GAN with a 3-layer MLP generator (128, 512, 128) with ReLU activations and a latent dimension of 10. We set the number of projections K to 50, the batch size to 50 and the learning rate to 3×10^{-3} . **Synthetic Multi-Task Density Estimation** We set the batch size to 150, and parametrize each measure ν_p as a discrete measure with 150 atoms which we optimize over. We set the number of projections to 20. **Earth Multi-Task Density Estimation** We set the batch size to 900 (full-batch), and parametrize each measure ν_p as a discrete measure with 900 atoms which we optimize over. We set the number of projections to 20. **Multi-Task Reinforcement Learning** The horizon is set to $T = 200$. The learning rate is set to 2.5×10^{-4} , and the batch size to optimize the Q -function to 32. The Q -network is a 1-layer MLP with tanh activation. We use $f(x) = e^{-5x}$ to rescale the reward function following Dadashi et al. (2020), and we set the number of projections to $K = 50$.